

# In Situ Quantification of the Local Electrocatalytic Activity via Electrochemical Scanning Tunneling Microscopy

Richard W. Haid, Regina M. Kluge, Yunchang Liang, and Aliaksandr S. Bandarenka\*

Identification of catalytically active sites at solid/liquid interfaces under reaction conditions is an essential task to improve the catalyst design for sustainable energy devices. Electrochemical scanning tunneling microscopy (EC-STM) combines the control of the surface reactions with imaging on a nanoscale. When performing EC-STM under reaction conditions, the recorded analytical signal shows higher fluctuations (noise) at active sites compared to non-active sites (noise-EC-STM or n-EC-STM). In the past, this approach has been proven as a valid tool to identify the location of active sites. In this work, the authors show that this method can be extended to obtain quantitative information of the local activity. For the platinum(111) surface under oxygen reduction reaction conditions, a linear relationship between the STM noise level and a measure of reactivity, the turn-over frequency is found. Since it is known that the most active sites for this system are located at concave sites, the method has been applied to quantify the activity at steps. The obtained activity enhancement factors appeared to be in good agreement with the literature. Thus, n-EC-STM is a powerful method not only to in situ identify the location of active sites but also to determine and compare local reactivity.

## 1. Introduction

The large-scale commercialization of sustainable electrochemical energy provision hinges on the discovery and improvement of appropriate electrocatalytic materials.<sup>[1]</sup> Especially the oxygen reduction reaction (ORR) has remained a significant roadblock due to its sluggish kinetics.<sup>[2,3]</sup> Taking place, inter alia, at the cathode of polymer–electrolyte membrane and direct-methanol fuel cells, the ORR is an imperative element of clean mobile energy generation.<sup>[4–6]</sup> However, even when using state of the art platinum (Pt) catalysts, the necessary overpotential to drive the reaction at a substantial rate is not sufficient for commercial com-

petitiveness. Neglecting mass transport limitations, the reaction rate is mainly governed by the binding of reaction intermediates to the catalyst surface, which should be neither too strong nor too weak. Consequently, the quality of a catalyst depends strongly on the amount of surface sites which offer optimal binding for reaction intermediates, that is, active sites. In this light, it is necessary to identify and evaluate the nature of these active electrocatalytic centers.<sup>[7–10]</sup>

In a real system, the catalyst surface will not be a homogeneous arrangement of identical surface sites and consequently, various distinctive adsorption sites are available for reaction intermediates. Their location and corresponding binding energies can be predicted by theoretical models, which have been demonstrated for both single crystal surfaces and nanoparticles.<sup>[11–16]</sup> For experimental confirmation of such predictions, special approaches, such as scanning photoelectrochemical microscopy, scanning electrochemical microscopy, or electrochemical scanning tunneling microscopy (EC-STM), that are able to in situ characterize catalytic systems and their active sites, are necessary.<sup>[17–19]</sup> Recently, EC-STM has been proven capable of visualizing active sites of several model systems by monitoring the noise level in the STM signal (n-EC-STM).<sup>[19–22]</sup> Due to a local increase in the relative noise level at active compared to non-active sites, this technique is able to render an activity map of the electrode surface. Moreover, different levels of activity can be distinguished by the extent of the recorded noise. Still, the results are so far only qualitative.

In this work, we propose a method that expands the capabilities of n-EC-STM from qualitative mapping of active sites to quantitative determination of the local surface activity. We use the well-studied example of Pt(111) as ORR catalyst in acidic media as a model system.<sup>[9,12,19,23–28]</sup> In a first step, we were able to linearly relate the intensity of the n-EC-STM noise to the electrocatalytic activity of a Pt(111) surface. In the second step, we estimated the local activity of concave sites at step edges of the Pt(111) single crystal. To this end, the noise levels at such a step site were determined for different potentials. In order to extract the corresponding activities, the linear noise-activity relation determined in the first step is used. As expected from theoretical predictions, step sites exhibit a superior activity compared to (111) terraces.<sup>[29]</sup> The enhancement factors of the activity at the steps compared to the terraces were determined and compared to literature. In this regard, the maximum observed activity increase coincides remarkably well with the Pt(221) facet, which is believed to be the most active for

trochemical microscopy, or electrochemical scanning tunneling microscopy (EC-STM), that are able to in situ characterize catalytic systems and their active sites, are necessary.<sup>[17–19]</sup> Recently, EC-STM has been proven capable of visualizing active sites of several model systems by monitoring the noise level in the STM signal (n-EC-STM).<sup>[19–22]</sup> Due to a local increase in the relative noise level at active compared to non-active sites, this technique is able to render an activity map of the electrode surface. Moreover, different levels of activity can be distinguished by the extent of the recorded noise. Still, the results are so far only qualitative.

R. W. Haid, R. M. Kluge, Dr. Y. Liang, Prof. A. S. Bandarenka  
Department of Physics (ECS)  
Technical University of Munich  
James-Franck-Straße 1, Garching 85748, Germany  
E-mail: bandarenka@ph.tum.de

Prof. A. S. Bandarenka  
Catalysis Research Center TUM  
Ernst-Otto-Fischer-Straße 1, Garching 85748, Germany

 The ORCID identification number(s) for the author(s) of this article can be found under <https://doi.org/10.1002/smt.202000710>.

© 2020 The Authors. Published by Wiley-VCH GmbH. This is an open access article under the terms of the Creative Commons Attribution License, which permits use, distribution and reproduction in any medium, provided the original work is properly cited.

DOI: 10.1002/smt.202000710

the ORR.<sup>[13]</sup> Still, the determination of the crystal facet of the examined steps eludes the capabilities of the n-EC-STM technique. Therefore, theoretical simulations are needed to fully harvest the benefits of quantitative n-EC-STM. We are confident that the quantitative assessment of electrode surface behavior under reaction conditions via n-EC-STM can offer valuable guidelines for the design of efficient electrocatalysts.

## 2. Results and Discussion

### 2.1. Noise Level-Activity Relation of Pt(111) Surfaces for the ORR

In this study, a Pt(111) single crystal in 0.1 M HClO<sub>4</sub> was investigated under the ORR conditions using n-EC-STM. For an

introduction of the technique please refer to the Experimental Section and the Supporting Information, where the interrelation of reactivity and noise level of the recorded STM signal are addressed in detail. Due to the cell design limitations imposed by the EC-STM set-up (see Figure S1, Supporting Information, for a sketch of the EC-STM cell), the choice of reference electrode (RE) is restricted. In order to avoid contamination of the sample surface, a Pt wire was employed as a quasi-reference electrode, which has already been demonstrated as a reliable option for EC-STM purposes, although a direct transfer to reversible hydrogen electrode (RHE) scale is not practicable.<sup>[19–22]</sup> Figure 1A shows the current density  $j_{WE}$  of the working electrode (WE) against different potentials in the ORR region. The curve indicates a steady increase in the current from 0.00 to –0.25 V versus Pt. At potentials lower than

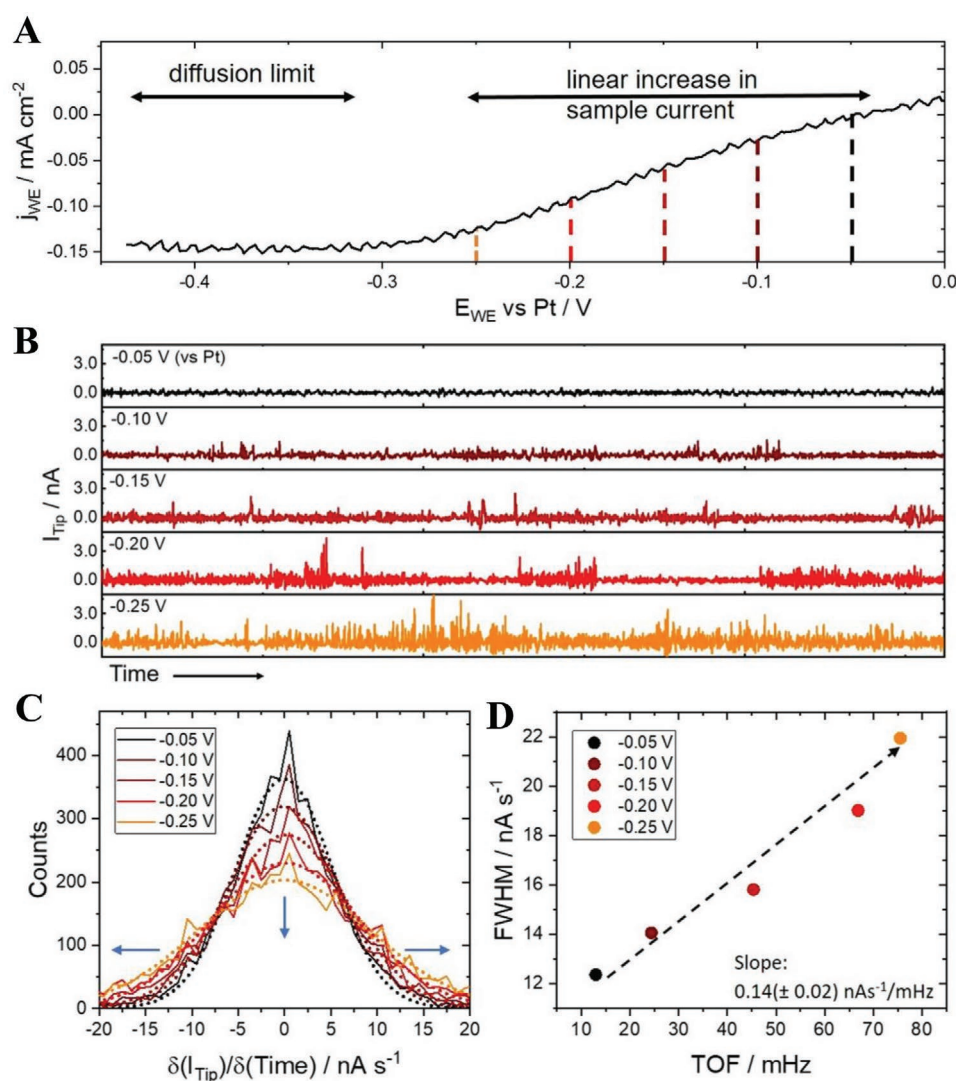


**Figure 1.** A) The cathodic scan of the ORR region of Pt(111) in 0.1 M HClO<sub>4</sub> (exposed to air). The data were recorded in the EC-STM setup using a Pt-quasi-reference electrode. The sample current has been normalized to the geometric area. The ORR current increases quasi-linearly until the mass transfer limitation at around –0.3 V versus Pt. B) The time-dependent change of the tunneling current at a (111) terrace site. Each sub-image refers to a single potential, as labeled and colored according to the color code. With decreasing potential, the noise level gets visibly higher. C) Histograms of the measurements in (B). A sharper curve corresponds to a lower noise level, and a broader and flatter one to a high noise level. Dotted lines represent Gaussian fits of the data. D) The FWHM of the Gaussians from (C) are plotted against the TOF<sub>r</sub>. The latter has been calculated from the sample current at the corresponding potential. The FWHM serves as a measure of the noise level. The resulting noise-activity relation shows a quasi-linear trend.

−0.3 V versus Pt, mass transport limits the current and the curve plateaus.

With this in mind, we recorded the tunneling current over time while maintaining the STM tip at a fixed position over a (111) terrace. For these measurements, the STM is operated in constant height mode, which due to the disabled feedback loop offers the highest accuracy. A wide terrace (>100 nm) ensures that the tip stays over a comparable surface site, even if the position is moved marginally by thermal drift during the measurement. In Figure 1B, an excerpt ( $\approx 2$  s) of the STM signal (tip current,  $I_{\text{Tip}}$ ) over time, is given at different potentials. For the full measurement, the STM signal was recorded for 128 s at each applied potential. As can be seen, decreasing the potential stepwise from −0.05 V versus Pt to −0.25 V versus Pt yields the expected increase in the noise level of the tunneling current. Histograms of the tip current are given in Figure 1C for each applied potential. The shape and height of the distribution reflect the extent of the noise. A high noise level in the STM signal leads to a broad and flat distribution of the tunneling current and vice versa a low noise level to a distinct peak of higher intensity. The dotted lines in Figure 1C represent Gaussian fits for each curve. The full width at half maximum (FWHM) of these Gaussian curves is used to represent the noise level of the measurements in a quantifiable way. Figure 1D plots the FWHM against the turn-over-frequency (TOF) at the corresponding potential. The TOF is a measure of the reaction rate and is defined as the number of electron transfers per surface site and per time unit. Since the exposed surface area and crystal structure of Pt(111) are known, the TOF can be calculated from the current density of the working electrode  $j_{\text{WE}}$  at any given potential. For this purpose, the working electrode current  $I_{\text{WE}}$ , was recorded chronoamperometrically and simultaneously to the EC-STM measurement. For details on the calculation of the TOF please refer to the Experimental Section and for the chronoamperometric measurements to Figure S2 and Table S1, Supporting Information. Since it has been shown that terrace sites are active towards the ORR,<sup>[19]</sup> the TOF of the whole sample is equal or close to the one of any given terrace site on the surface ( $\text{TOF}_t$ ). Due to the high activity of step sites, a concern might be that the overall activity of the sample is dominated by these sites and that the  $\text{TOF}_t$  might be miscalculated. However, according to Kibler et al., the employed preparation technique should yield a low number of steps, leading to the conclusion that the overall activity is predominantly governed by terraces.<sup>[30]</sup> In Figure S3, Supporting Information, the cyclic voltammogram (CV) of the Pt(111) crystal is given and compared to the literature. Although the step density on the Pt(111) surface cannot be exactly calculated, STM scans of the surface indicated that the Pt(111) surface investigated here is well-defined and yields a low defect density (see Figure S4, Supporting Information). Therefore, recording and quantifying the noise level over an extended (111) terrace should allow to directly relate the observed STM signal to the  $\text{TOF}_t$  at the applied potential. We find a linear FWHM-TOF correlation with a slope of  $0.14 (\pm 0.02) \text{ nA s}^{-1} \text{ mHz}^{-1}$ . Evidently, sample activity (TOF) and noise level (FWHM) in this model system are linearly related and an increase in reaction rate will lead to proportionally higher fluctuations in the tunneling current. We recognize that the tip itself might affect the electrocatalytic

processes in its vicinity (due to convection differences, electric field, etc.); however, by only comparing the relative noise levels and by averaging the TOF over the whole sample surface, these issues should be insignificant.

Repetition of the experiment leads to similar results (Figure S5, Supporting Information); however, the absolute values obtained for the slope and offset of the linear relation varied between the measurements. We can identify several origins of these discrepancies. First, the sample surface was freshly prepared prior to each measurement, leading to minor variations in the surface quality, which could impact the TOF calculated from the sample current. The number and thus activity of the terrace sites may then be slightly overestimated and offset the linear relation. Secondly, the electrolyte in the EC-STM cell was exposed to air and subject to drying over time. This can influence the concentrations and may shift or tilt the relation slightly, although no noticeable influence was observed, when reversing the order of the potential steps (see Supporting Information). Most importantly, the tip shape and insulation influence the measurements. A broader tip may pick up an overall higher or lower noise level than a sharper one. A similar effect can be expected from the insulation of the tip. A well-insulated tip will be more precise, whereas a larger exposed tip area may lead to a generally enhanced noise level. However, several supplementary experiments (Figure S6, Supporting Information) proved that none of these technical aspects should change the overall linear trend, merely regulate its characteristics. For the listed reasons, it is unfortunately not possible to determine a unifying parameter to describe the relation, but a reproducibly linear trend was revealed. Moreover, for a completely controlled system, the relation should be true at any point of the sample surface. In consequence, it should be possible to render a calibration curve from a well-defined surface to obtain the sample-specific noise level-activity relation and apply it to measure the activity of other surface structures. In the following, the local activity of a step edge will be determined using a nearby (111) terrace for calibration.

## 2.2. Determining the Local ORR Activity of Pt(111) Step Sites

Motivated by the previous investigations, we exploited the discovered linear relation between the noise level and the ORR activity to elicit the TOF of some step sites ( $\text{TOF}_s$ ) on the Pt(111) surface. Due to the sensitivity of the absolute values of the slope and the offset of the linear relation on the n-EC-STM system, it is crucial to record the n-EC-STM data for both terrace and step within one measurement, for example shown in Figure 2A. The measurements were conducted in the constant current mode, to access the surface structure. In this case, the particular focus lies on the terrace to the left of the step, which will serve as calibration data for the analysis. Already from Figure 2A, an increase in noise level with decreasing potential is easily recognizable. The noise level near the step is more dominant than on the flat terraces, indicating that the step is more active than the terrace. These experimental observations are in line with previous investigations as well as theoretical predictions.<sup>[21,29]</sup>

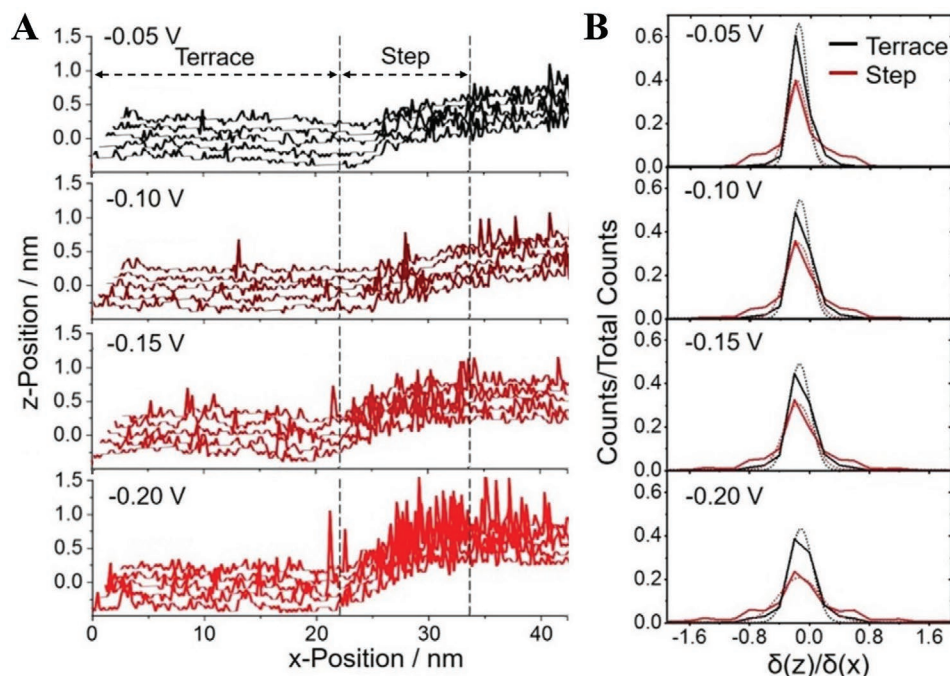


**Figure 2.** A) n-EC-STM measurement of a Pt(111) step and adjacent terraces. With decreasing potential, the overall noise level increases. This increase is most pronounced near the step edge as can be seen from the higher and denser spikes in the signal. For data evaluation, the terrace data (on the left) will be used as calibration for the relation between noise level and activity on this sample. B) Histograms after separating the data for terrace (black) and step (red). To make the distributions comparable, counts are normalized to the total number of counts for each area. At every applied sample potential, the step shows a higher noise level relative to the terrace, as evident from the broader and less intense distribution. All potentials given are referred to the Pt quasi-reference electrode.

Histograms of the height profile for the terrace and step data, respectively, are given in Figure 2B. Data are divided into the “step” and “terrace” as by the dotted lines in Figure 2B. The descriptor of the noise level of both step ( $\text{FWHM}_s$ ) and terrace ( $\text{FWHM}_t$ ) is acquired from Gaussian fits of the histograms. We obtain a linear noise level–activity relation between the  $\text{FWHM}_t$  and the calculated TOF of the terrace ( $\text{TOF}_t$ ).

The latter is again obtained from the overall sample current  $j_{WE}$ . The relation between  $\text{TOF}_t$  and  $\text{FWHM}_t$  should then be true for any structure on the sample surface and thus serves as a noise level–activity calibration curve (Figure 3A) for this particular measurement. We state as a side note that the linear trend between  $\text{FWHM}$  and TOF can evidently be obtained in both constant current and constant height mode. As the last

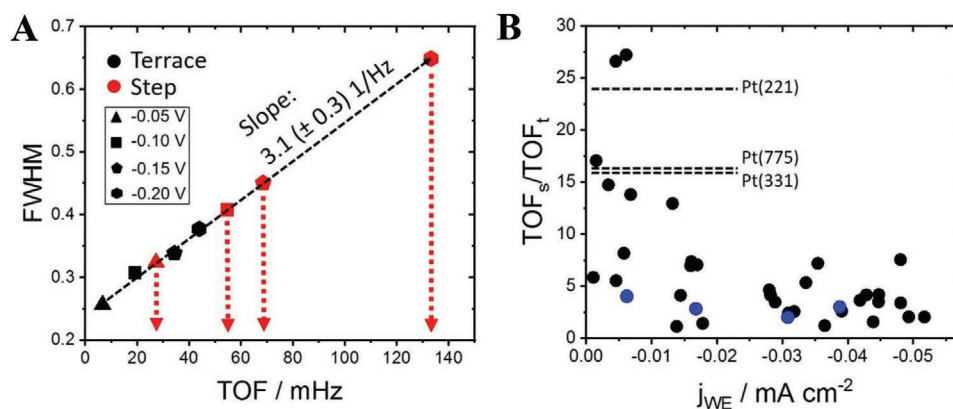


**Figure 3.** A) In order to extract the local activity at the step, a linear calibration curve (dotted line) is fitted to the terrace data (black), relating the noise level ( $\text{FWHM}$ ) to the activity (TOF). The latter has been determined from the overall sample current at the respective potential (see symbols; all recorded against a Pt quasi-reference). The  $\text{FWHM}_s$  of the step data (red) is placed on the curve to extrapolate the corresponding  $\text{TOF}_s$ . B) The enhancement factors  $\text{TOF}_s/\text{TOF}_t$  at each applied potential are plotted against the  $j_{WE}$  recorded during the experiment. Data points from (A) are displayed in blue. The other points originate from similar measurements given in Figure S7, Supporting Information. The highest recorded factors are close to the best performing concave sites at the high-index planes of Pt for the ORR (Pt(221), Pt(775), Pt(331)), as indicated in the graph.<sup>[29,31]</sup> Especially at  $j_{WE}$  close to zero, the steps generate significantly higher activity than the terrace. Details of the here displayed data can be found in Table S2, Supporting Information.

step, the FWHM values for the step sites ( $\text{FWHM}_s$ ) are placed on this linear relation, and the corresponding  $\text{TOF}_s$  is extrapolated for each applied potential. Repetition of the experiment at several comparable step sites led to similar results, which are summarized in Figure S7, Supporting Information.

Following these investigations, we can directly compare the activities of the terrace and the step, by calculating the factor  $\text{TOF}_s/\text{TOF}_t$  for each applied potential (e.g.,  $(\text{TOF}_s \text{ at } -0.05 \text{ V versus Pt})/(\text{TOF}_t \text{ at } -0.05 \text{ V versus Pt})$ ). In Figure 3B, all the obtained activity enhancement factors from nine measurement series (see Figure S7, Supporting Information) are collected, with the data from Figure 3A highlighted in blue. They are plotted against the sample current density  $j_{\text{WE}}$  measured during the experiment, which serves as a descriptor for the overall activity of the sample. Details of the data points can be found in Table S2, Supporting Information. Enhancement factors between 1 and 27 have been observed, their spread decreasing with increasing negative  $j_{\text{WE}}$ . The observed steps were of various heights and orientations, which is expected to influence their activity towards the ORR.<sup>[26,29,31–33]</sup> However, detailed characterization of their nature was not possible with EC-STM for this type of the sample at room temperature in contact with the electrolyte. We can assume that steps of several orientations are represented within the recorded data.

The enhancement factors can be discussed by comparing their activity enhancement with that of stepped Pt crystals, examined with rotating disk electrode (RDE) measurements.<sup>[26,29,31–33]</sup> We need, however, to keep in mind that the TOF given here is defined as the number of charge transfers per site and time, as measured in the EC-STM set-up. It differs from the RDE activity by not being mass transport corrected and not taking place in  $\text{O}_2$ -saturated atmosphere. The comparison to RDE activity can nonetheless serve as a valuable test for our method.

Noticeably, at lower sample activities, which are typically used for RDE measurements, the step seems to reach a proportionally higher reaction rate. The maximal enhancement factor we observed is around 27, which agrees well with the improvement that would be expected from the most active concave sites at Pt(221), in comparison to the flat Pt(111). The reported activity for the Pt(221) facet is around 6.2 times higher than the (111) surface; taking the terrace width of four atoms into account, gives a total enhancement factor of 24.8 for the concave step site.<sup>[29,31]</sup> The next highest differences we recorded were at a factor of around 16. Based on the alluded studies, these could be related to the Pt(775) or Pt(331) facet. The majority of the enhancement factors seem to lie between 1 and 10. They can be attributed to the many other high-index planes that have a slightly improved activity over the (111) surface.<sup>[32,33]</sup> Towards lower potentials (higher  $j_{\text{WE}}$ ), the enhancement factors are not that distinct anymore. A possible explanation for this could be found in the influence of kinetic and mass transport effects. The limit for the step might already be reached at higher potentials (lower negative  $j_{\text{WE}}$ ) than for terraces, while the activity of the latter is still increasing. This would lead to a diminished difference in the activities of step and terrace.

In summary, we were able to employ n-EC-STM to quantify the activity of Pt(111) surface structures. The resulting enhancement factors between the step and the terrace sites

agree remarkably well with expected values of typical Pt facets based on the literature data. The experimental conditions were imitated as closely as the restrictions in the EC-STM allowed. Despite the different experimental methods, the close match between our results and these previous studies supports the functionality of the n-EC-STM measurements. However, unlike RDE measurements, the n-EC-STM technique offers the possibility to probe specific surface features with a high spatial resolution. The major drawback of this technique is the sensitivity with regards to the technical aspects such as tip shape and electrolyte concentration. For this reason, the dependencies must always be taken in regard to a well-defined reference point. Moreover, since n-EC-STM does not allow precise characterization of, for example, steps in the investigated model system, supplementary experiments and methods have to be consulted to interpret the results. We argue, however, that this technique can be a valuable piece of the puzzle when analyzing the activity of catalytic materials, as it can be applied in situ and allows to locally access the activity of structures deviating from well-defined surfaces. With this in mind, it should be possible to extend this method to “quantify” other reactions and surfaces. Moreover, it could be of interest to test the method at other surface structures such as defects or foreign materials deposited on a catalyst surface.

### 3. Conclusion

In this work, we elaborated a new method for the in situ quantification of the electrocatalytic activity using the n-EC-STM technique. We related the recorded noise, originating from the ORR at a well-defined active site on the Pt(111) surface to the corresponding TOF calculated from the sample current. We found a linear correlation between the noise and activity levels, indicating a direct link between the fluctuations in the STM signal over an active site and the rate of the reaction. The absolute values of the relation were observed to be dependent on several technical aspects of the measurement. This insight was applied to obtain the local activity of step sites by evaluating the noise level with regard to an adjacent terrace. Results showed remarkable accordance with reported activity improvements obtained from stepped single crystals in the RDE measurements. We conclude that this approach can be utilized for direct quantification of activity in a highly localized area, enabling the in situ characterization of specific surface sites.

### 4. Experimental Section

*The Concept of n-EC-STM Measurements:* The n-EC-STM technique utilizes a conventional STM in an electrochemical environment to observe an electrode surface under reaction conditions. The four-electrode setup comprised of tip, sample (WE), RE, and counter electrode (CE) is connected to a bipotentiostat controlling both tip and sample voltage, each against the RE. Manipulation of the WE potential regulates the occurrence and rate of reactions at the electrode–electrolyte interface. It has been recognized that the effective tunneling barrier is strongly influenced by the molecules within the gap between tip and sample.<sup>[34–37]</sup> Therefore, if the potential is held at a value which enables a reaction (reaction “On”), two scenarios have to be distinguished. If the tip is placed over a non-active site, the tunneling

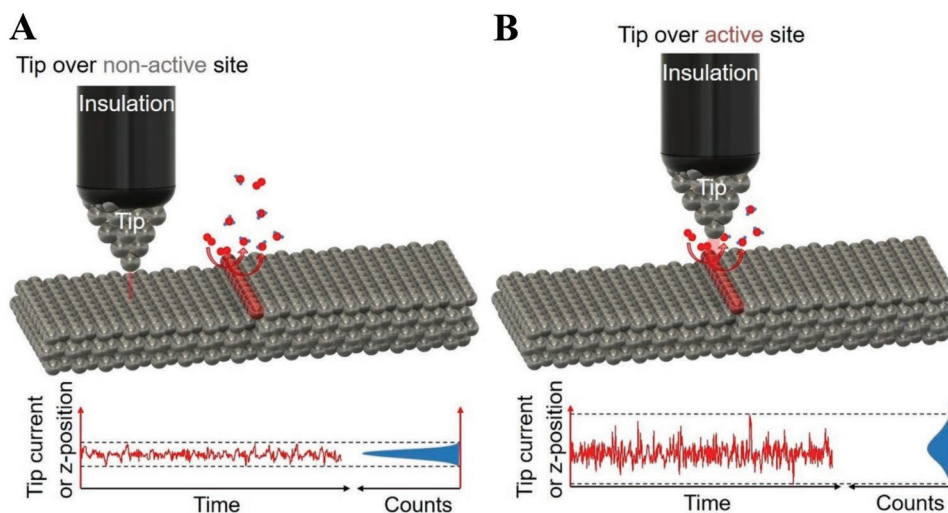


**Figure 4.** The concept of n-EC-STM measurements. The potential of the sample is set such that a reaction occurs at the surface. A) Over a non-active site (gray), the tunneling medium is stable and the STM response depends only on the electronic structure of the surface. Therefore, the recorded STM signal (tunneling current or height profile; red) should be almost constant and yield a narrow distribution (blue). B) Over an active site (red), the reaction processes disturb the tunneling barrier, which is reflected as noise in the STM signal. In this case, the recorded STM signal is fluctuating and yields a broadened distribution.

barrier is essentially constant at this position (Figure 4A). In this case, recording the tunneling current over time will yield a nearly constant value. Note that the recorded STM signal can either be the tip current in the constant height mode or the z-position of the tip in the constant current mode. For convenience, only “recorded signal” or “STM signal” will be referred to, in this section. By contrast, if the tip is placed over an active site, the reaction processes occurring in the gap between tip and sample will influence the STM signal (Figure 4B). As can be seen in the more detailed sketch in Figure S8, Supporting Information, the molecules and their orientation within the tunneling barrier changes significantly. As previously mentioned, this will lead to a continually alternating tunneling current which is reflected as noise in the STM signal. As a means for the quantification of the noise level, the derivative of the tip current over time is calculated. Consequently, a frequency-count is performed, leading to a histogram of the noise level. Effectively this means, that a narrow distribution can be expected for measurements with small changes in the tunneling current, whereas a broad distribution is related to higher noise levels. These histograms are fitted with a Gaussian and its FWHM is used as a descriptor for the noise level. This signifies that a small FWHM corresponds to a low noise level, while a large FWHM reflects a high noise level in the tunneling current.

The activity of any surface site is given by the amount of reactions occurring within a certain timeframe. In this study, the TOF was selected for this purpose; it is defined as the number of reactions per second per active site. For this experimental set-up, the TOF of the whole sample at any given potential can be calculated from the current density since this gives essentially the number of electrons transferred through the sample per second:

$$\text{TOF} = \frac{|j_{\text{WE}}| A_{\text{S}}}{ne N_{\text{a}}} \quad (1)$$

where  $j_{\text{WE}}$  is the sample current density,  $A_{\text{S}}$  the exposed surface area of the sample in the STM sample holder (0.126 cm<sup>2</sup>),  $n$  the number of electrons transferred during the reaction (for ORR:  $n = 4$ ),  $e$  the elemental charge, and  $N_{\text{a}}$  the number of surface atoms. The latter can be estimated using  $A_{\text{S}}$  and the lattice parameters of Pt(111) ( $a_{\text{d}} = 2.83 \text{ \AA}$ ,  $\alpha = 60^\circ$ ):<sup>[38]</sup>

$$N_{\text{a}} = \frac{A_{\text{S}}}{a_{\text{d}}^2 \sin(\alpha)} \quad (2)$$

Experiments in this study were performed in a MultiMode EC-STM/EC-AFM scanning probe microscope (Veeco Instruments) connected to a NanoScope III scan feedback controller and a Universal Bipotentiostat (Veeco Instruments). The STM tips were mechanically cut/ripped from a Pt80Ir20 wire (GoodFellow,  $\varnothing = 0.25 \text{ mm}$ ). To prevent unwanted reactions at the tips, they were insulated using Apiezon wax.<sup>[39]</sup> The Pt single crystal was mounted on a specifically designed sample holder, comprised of a stainless steel base plate and a Teflon ring connected by screws. Reference and counter electrodes (both Pt wires, MaTeck,  $\varnothing = 0.5 \text{ mm}$ ) were immersed into the electrolyte close to the STM probe. Experiments were conducted at room temperature and the cell was exposed to air at all times. For the measurements in Section 2.1, the current set-point of the (EC-) STM was 2 nA, the scan rate 4 Hz, and the tip potential  $-0.05 \text{ V}$  versus Pt. For Section 2.2, the respective parameters were set to 1.5 nA, 1.5 Hz, and 0.00 V versus Pt.

**Sample Preparation:** The glass cell for preparation of the single crystal was cleaned using Caro’s acid (3:1 mixture of H<sub>2</sub>SO<sub>4</sub> and H<sub>2</sub>O<sub>2</sub>) and afterward flushed with boiling, ultrapure water (18.2 M $\Omega$ , Evoqua, Germany). As RE, a mercury-mercurous sulfate electrode (MMS, SI Analytics, Germany) was employed and connected to the main cell by a Luggin capillary filled with 0.1 M HClO<sub>4</sub> (Suprapur, Merck Germany). The potentials were subsequently converted to the RHE scale via  $U(\text{RHE}) = U(\text{MMS}) + 0.72 \text{ V}$ . A Pt-wire served as CE (MaTeck,  $\varnothing = 0.5 \text{ mm}$ ). The potential was controlled by a VSP-300 potentiostat (Bio-Logic, France) using the accompanying EC-Lab software (V11.30).

The Pt(111) single crystal ( $\varnothing = 0.5 \text{ mm}$ ; MaTeck, Germany) was prepared according to the method proposed by Kibler et al.<sup>[30]</sup> It was electrochemically cleaned and subsequently annealed in an isobutane flame. During the cooling, it was kept in an Ar/CO atmosphere (1000 ppm CO 4.7, and Ar 5.0; both Air Liquide, Germany) to protect the surface. To ensure satisfying surface quality, a cyclic voltammogram in Ar-saturated 0.1 M HClO<sub>4</sub> (Figure S3, Supporting Information) was evaluated after the annealing process. Comparing the obtained shape and features to literature guarantees the existence of the Pt(111) surface structure.<sup>[30,40,41]</sup>

**Data Evaluation:** The data were evaluated using WSxM 5.0 Develop 9.1, Origin 2018b, and Python 2.7.<sup>[42]</sup>

## Supporting Information

Supporting Information is available from the Wiley Online Library or from the author.

## Acknowledgements

R.W.H. and R.M.K. contributed equally to this work. The authors kindly acknowledge the financial support from German Research Foundation (DFG) under Grant No. 355784621, under Germany's Excellence Strategy-EXC 2089/1-390776260, under Germany's Excellence cluster "e-conversion" and DFG projects BA 5795/4-1 and BA 5795/3-1 and TUM IGSSE, project 11.01.

Open access funding enabled and organized by Projekt DEAL.

## Conflict of Interest

The authors declare no conflict of interest.

## Keywords

active sites, electrocatalysis, electrochemical scanning tunneling microscopy, oxygen reduction reaction, Pt(111)

Received: August 11, 2020

Revised: September 10, 2020

Published online:

- [1] Z. W. Seh, J. Kibsgaard, C. F. Dickens, I. Chorkendorff, J. K. Nørskov, T. F. Jaramillo, *Science* **2017**, 355, eaad4998.
- [2] I. Katsounaros, S. Cherevko, A. R. Zeradjanin, K. J. J. Mayrhofer, *Angew. Chem., Int. Ed.* **2014**, 53, 102.
- [3] I. E. L. Stephens, A. S. Bondarenko, U. Grønbjerg, J. Rossmeisl, I. Chorkendorff, *Energy Environ. Sci.* **2012**, 5, 6744.
- [4] S. Sui, X. Wang, X. Zhou, Y. Su, S. Riffat, C.-j. Liu, *J. Mater. Chem. A* **2017**, 5, 1808.
- [5] M. Shao, Q. Chang, J.-P. Dodelet, R. Chenitz, *Chem. Rev.* **2016**, 116, 3594.
- [6] A. S. Aricò, S. Srinivasan, V. Antonucci, *Fuel Cells* **2001**, 1, 133.
- [7] J. Kibsgaard, Z. Chen, B. N. Reinecke, T. F. Jaramillo, *Nat. Mater.* **2012**, 11, 963.
- [8] B. Garlyyev, J. Fichtner, O. Piqué, O. Schneider, A. S. Bandarenka, F. Calle-Vallejo, *Chem. Sci.* **2019**, 10, 8060.
- [9] A. S. Bandarenka, H. A. Hansen, J. Rossmeisl, I. E. L. Stephens, *Phys. Chem. Chem. Phys.* **2014**, 16, 13625.
- [10] P. Strasser, M. Gliech, S. Kuehl, T. Moeller, *Chem. Soc. Rev.* **2018**, 47, 715.
- [11] J. K. Nørskov, T. Bligaard, B. Hvolbæk, F. Abild-Pedersen, I. Chorkendorff, C. H. Christensen, *Chem. Soc. Rev.* **2008**, 37, 2163.
- [12] V. Tripkovic, E. Skúlason, S. Siahrostami, J. K. Nørskov, J. Rossmeisl, *Electrochim. Acta* **2010**, 55, 7975.
- [13] J. Rossmeisl, G. S. Karlberg, T. Jaramillo, J. K. Nørskov, *Faraday Discuss.* **2009**, 140, 337.
- [14] J. Yue, Z. Du, M. Shao, *J. Phys. Chem. Lett.* **2015**, 6, 3346.
- [15] F. Calle-Vallejo, J. Tymoczko, V. Colic, Q. H. Vu, M. D. Pohl, K. Morgenstern, D. Loffreda, P. Sautet, W. Schuhmann, A. S. Bandarenka, *Science* **2015**, 350, 185.
- [16] M. Rück, A. S. Bandarenka, F. Calle-Vallejo, A. Gagliardi, *J. Phys. Chem. Lett.* **2018**, 9, 4463.
- [17] J. Y. Lee, S. Kang, D. Lee, S. Choi, S. Yang, K. Kim, Y. S. Kim, K. C. Kwon, S. H. Choi, S. M. Kim, J. Kim, J. Park, H. Park, W. Huh, H. S. Kang, S. W. Lee, H.-G. Park, M. J. Ko, H. Cheng, S. Han, H. W. Jang, C.-H. Lee, *Nano Energy* **2019**, 65, 104053.
- [18] X. Chen, A. Maljusch, R. A. Rincón, A. Battistel, A. S. Bandarenka, W. Schuhmann, *Chem. Commun.* **2014**, 50, 13250.
- [19] J. H. Pfisterer, Y. Liang, O. Schneider, A. S. Bandarenka, *Nature* **2017**, 549, 74.
- [20] Y. Liang, D. McLaughlin, C. Csoklich, O. Schneider, A. S. Bandarenka, *Energy Environ. Sci.* **2019**, 12, 351.
- [21] Y. Liang, C. Csoklich, D. McLaughlin, O. Schneider, A. S. Bandarenka, *ACS Appl. Mater. Interfaces* **2019**, 11, 12476.
- [22] E. Mitterreiter, Y. Liang, M. Golibrzuch, D. McLaughlin, C. Csoklich, J. D. Bartl, A. Holleitner, U. Wurstbauer, A. S. Bandarenka, *npj 2D Mater. Appl.* **2019**, 3, 25.
- [23] N. M. Marković, R. R. Adžić, B. D. Cahan, E. B. Yeager, *J. Electroanal. Chem.* **1994**, 377, 249.
- [24] M. Wakisaka, H. Suzuki, S. Mitsui, H. Uchida, M. Watanabe, *Langmuir* **2009**, 25, 1897.
- [25] N. M. Markovic, H. Gasteiger, P. N. Ross, *J. Electrochem. Soc.* **1997**, 144, 1591.
- [26] A. M. Gómez-Marín, R. Rizo, J. M. Feliu, *Catal. Sci. Technol.* **2014**, 4, 1685.
- [27] A. S. Bondarenko, I. E. L. Stephens, H. A. Hansen, F. J. Pérez-Alonso, V. Tripkovic, T. P. Johansson, J. Rossmeisl, J. K. Nørskov, I. Chorkendorff, *Langmuir* **2011**, 27, 2058.
- [28] A. M. Gómez-Marín, J. M. Feliu, *ChemSusChem* **2013**, 6, 1091.
- [29] F. Calle-Vallejo, M. D. Pohl, D. Reinisch, D. Loffreda, P. Sautet, A. S. Bandarenka, *Chem. Sci.* **2017**, 8, 2283.
- [30] L. A. Kibler, *Preparation and Characterization of Nobel Metal Single Crystal Electrode Surfaces*, International Society of Electrochemistry **2003**.
- [31] A. Kuzume, E. Herrero, J. M. Feliu, *J. Electroanal. Chem.* **2007**, 599, 333.
- [32] N. Hoshi, M. Nakamura, A. Hitotsuyanagi, *Electrochim. Acta* **2013**, 112, 899.
- [33] V. Čolić, A. S. Bandarenka, *ACS Catal.* **2016**, 6, 5378.
- [34] J. Halbritter, G. Repphun, S. Vinzelberg, G. Staikov, W. J. Lorenz, *Electrochim. Acta.* **1995**, 40, 1385.
- [35] M. Hugelmann, W. Schindler, *Surf. Sci.* **2003**, 541, L643.
- [36] M. Hugelmann, W. Schindler, *J. Electrochem. Soc.* **2004**, 151, E97.
- [37] F. C. Simeone, D. M. Kolb, S. Venkatchalam, T. Jacob, *Angew. Chem. Int. Ed.* **2007**, 46, 8903.
- [38] K. Krupski, M. Moors, P. Jóźwik, T. Kobiela, A. Krupski, *Materials* **2015**, 8, 2935.
- [39] L. A. Nagahara, T. Thundat, S. M. Lindsay, *Rev. Sci. Instrum.* **1989**, 60, 3128.
- [40] J. X. Wang, N. M. Markovic, R. R. Adzic, *J. Phys. Chem. B* **2004**, 108, 4127.
- [41] L. Jacobse, Y. Huang, M. T. M. Koper, *Nat. Mater.* **2018**, 17, 277.
- [42] I. Horcas, R. Fernández, *Rev. Sci. Instrum.* **2007**, 78, 013705.